EFFECT OF SULFUR ON SIDEROPHILE ELEMENT PARTITIONING BETWEEN OLIVINE AND MARTIAN MANTLE PRIMARY MELT

Revision 1.1

Tomohiro Usui[1,2,5], Kevin Righter[2,5], Charles K. Shearer[3,4], and John H. Jones[4],

[1] Institute of Space and Astronautical Sciences, Japan Aerospace Exploration Agency, Kanagawa, 252-5210, Japan

[2] NASA Johnson Space Center, Mailcode XI2, 2101 NASA Pkwy, Houston, TX 77058

[3] Institute of Meteoritics, University of New Mexico, Albuquerque, NM 87131

[4] Lunar and Planetary Institute, 3600 Bay Area Blvd., Houston, TX 77058

[5] These authors contributed equally to this work

Abstract - Ni and Co variations in primary martian magmas exhibit anomalous incompatible behavior, which has remained an unexplained conundrum. Because martian magmas are S-rich, and some trace metals have reported enhanced solubility in S-bearing magmas, we have carried out a series of experiments to evaluate the effect of high-S melts on the olivine/melt partitioning of Ni, Co, Mn, V, and Cr. Near-liquidus experiments on a synthetic primary martian mantle melt (Yamato-980459 [Y98]) were completed in a piston cylinder apparatus at 0.75 GPa. Previous studies in S-free systems illustrate that the partition coefficients for these elements are dependent chiefly on $D(Mg)_{ol/melt}$ (the partition coefficient defined as wt% Mg in olivine / wt% Mg in melt), a proxy for temperature, and were used to calibrate a predictive expression that includes the effects of temperature [i.e., $D(Mg)_{ol/melt}$], melt composition, and oxygen fugacity. These predictive expressions are then used to isolate any effect in D(M) olivine/melt due to dissolved sulfur. The results show that S might have a small effect for Co, but not enough to change Co partitioning from compatible to incompatible in our experiments. Addition of a sulfur term to the D(Co) predictive expressions shows that nearly 8000 ppm of sulfur would be required in the melt (at liquidus temperature of Y98) for D(Co) to become <1. These S contents are 2 times higher than those of a sulfide saturated melt at the (P,T) conditions of a martian mantle source region. Therefore, the anomalous incompatible behavior observed in these primary magma suites must be due to another mechanism. High temperature, oxygen fugacity, and diffusion are not viable mechanisms, but magma mixing, assimilation, or kinetic crystallization effects remain possibilities.

Keywords: shergottite; olivine; transition metals; sulfur; basaltic magma

Introduction

First-row transition elements (FRTE, including Mn, Ni, Co, Fe, V, and Cr) are useful indicators of primary planetary mantle melts (Sato, 1976; Wänke and Dreibus, 1986) and the source mineralogy of mantle melts (Sobolev et al., 2007), and their ratios can be used to infer source heterogeneities in mantle-derived melts (e.g. Fe/Mn; Humayun et al., 2004; LeRoux et al., 2011). Since olivine is a common early-crystallizing phase in basaltic magmas that have produced planetary and asteroidal crusts, a number of experimental studies have investigated elemental partitioning between olivine and silicate melt (e.g., Toplis, 2005; Libourel, 1999; Jones, 1995). In particular, olivine/melt partition coefficients of Ni and Co (D(Ni) and $D(Co)_{ol/melt}$) have been intensively studied because these elements are preferentially partitioned into olivine and thus provide a uniquely useful insight into the basalt petrogenesis (e.g., Takahashi, 1978; Beattie et al., 1991; Longhi et al., 2010). Ni and Cr have both been used as indicators of primary melts of planetary mantles (e.g., Sato, 1977; Wänke and Dreibus, 1986; Sobolev et al., 2007). Vanadium partitioning between olivine and melt is sensitive to changes of oxygen fugacity and has been used as an oxybarometer (Shearer et al., 2006; Mallmann and O'Neill, 2013; Lee et al., 2003; Canil and Fedortchouk, 2001; Nakada et al. 2020). Chromium partitioning between olivine and melt is also dependent upon oxygen fugacity since Cr^{2+} is stable in melts at low fO_2 (e.g., Hanson and Jones, 1998). Finally, Mn partitioning differences between peridotite and pyroxenite can be used to place constraints on sources of mantle melts (LeRoux et al., 2011; Sobolev et al., 2007). Fe/Mn ratios in meteorites are used to trace the origins of various meteorite groups due to the variable volatility of Mn in the solar system (e.g., Papike, 1998; Goodrich and Delaney, 2000; Karner et al., 2003), but a comprehensive interpretation of this ratio must include an understanding of differences in olivine melt

69 partitioning for Fe and Mn. Overall, the FRTE are very useful in delineating source
70 characteristics and origin of planetary basalts.

71 Extensive studies of olivine/melt partitioning of FRTE have demonstrated the role of
72 pressure, temperature, oxygen fugacity, and melt composition in controlling the magnitude of D
73 (olivine/melt) (e.g., Takahashi, 1978; Beattie et al., 1991; Matzen et al., 2013; Longhi et al.,
74 2010; Elardo et al., 2011; Hanson and Jones, 1998; Mallmann and O'Neill, 2013; LeRoux et al.,
75 2011; Filiberto et al., 2009). Despite the many studies carried out on the partitioning behavior
76 of Ni and Co, basic chemical trends in terrestrial and planetary samples remain unexplained. For
77 example, Co exhibits incompatible behavior in olivines from Martian meteorites and lunar
78 basalts, while Ni exhibits compatible behavior **(Figure 1;** Papike et al. 2009; Usui et al., 2008;
79 Karner et al., 2003). High temperatures (~ 2000 °C) might be the cause of the opposite behavior
80 of Ni and Co as shown by Longhi et al. (2010) and Elardo et al. (2011) for lunar magma ocean
81 conditions, but these temperatures are much higher than liquidus temperatures of the olivine-
82 phyric shergottites, near 1500 °C at 0.5 GPa (e.g., Rapp et al., 2013) and therefore cannot be the
83 cause of the incompatible behavior. Similarly, Ni and Co exhibit de-coupled behavior in
84 terrestrial peridotite and pyroxenite, compared to their expected compatible behavior (Sobolev et
85 al., 2007; Herzberg et al., 2016).

86 A distinctive aspect of martian magmas and shergottites that might provide an
87 explanation for compatible Ni and incompatible Co is the high S contents of primitive shergottite
88 liquids (up to 2700 ppm; Franz et al., 2014). Sulfur is known to enhance the solubility of some
89 trace metals in terrestrial magmas. For example, chemical analyses of S-rich Mid-Ocean Ridge
90 Basalt (MORB) samples (i.e. un-degassed with respect to sulfur) suggest that S dissolved in
91 silicate melts can reduce $D(Ni)_{ol/melt}$ up to 50 % compared to S-free experimental systems (Li et

al., 2003). MORB glasses typically contain ~ 1000 ppm S at 8% MgO (e.g. Le Voyer, et al., 2019), and even at those concentration levels, S has a discernable effect on D(Ni) olivine/melt. Martian basaltic melts are known to contain even higher S contents (up to 2700 ppm; Dreibus et al., 1982, 2000; Zipfel et al., 2000; Shirai and Ebihara, 2004; Franz et al., 2014). The high S contents of shergottites in general as well as the high solubility of S in primitive shergottite melts (up to 4000 ppm; Righter et al., 2009) implies that S might be responsible for significantly influencing the Ni, Co, and other FRTE partitioning in shergottite olivines. Although Mn, V, and Cr all exhibit incompatibility in olivine for martian magmatic conditions (e.g., Karner et al., 2007; Righter et al., 2006; Hanson and Jones, 1998), the extent of their incompatibility (e.g. Mn in Herd et al., 2009) must be explored in S-bearing systems. Existing experimental data are not ideal for evaluating these effects for martian melt compositions at martian mantle and magmatic conditions. There are some studies that utilized S-bearing melts, but do not include martian compositions (e.g. Tuff et al., 2010), or have been carried out at low PT conditions that are not directly relevant to martian melt generation (e.g., Gaetani and Grove, 1997). Thus, the relevant set of P-T-fO_2 conditions and melt compositions have not yet been explored together in one study, and utilizing literature data would require extrapolation of one or more variables.

To explore the possible effects of S on the olivine/melt partitioning behavior of Ni, Co, Mn, V, and Cr, we have conducted experiments to examine partitioning between olivine and Martian primary mantle melt at Martian magmatic conditions (give P, T, fO_2) and variable and high S contents (up to 3000 ppm). Conditions of Martian magma genesis have been explored by several studies, and multiple saturation is thought to occur from 0.8 to 2 GPa and 1450 to 1575 °C (e.g., Rapp et al., 2013; Collinet et al., 2015; Filiberto et al., 2010; Gross et al., 2011). Given the known negative pressure dependence of sulfide saturation and S solubility in melts (Righter

et al. 2009; Holzheid and Grove, 2002), we chose the low pressure end of this range to allow the maximum values of S solubility - up to ~3000 ppm. In addition, oxygen fugacity was defined below the FMQ (fayalite-magnetite-quartz) buffer which is an appropriate value for the Martian mantle. The most primitive, unfractionated mantle melts are thought to be the olivine-phyric shergottites high MgO (15-20 wt%) and relatively low Al_2O_3 (<7 wt%). Therefore we chose the Yamato-980459 olivine-phyric shergottite as a starting composition for the experiments; this sample has also been featured in studies of Ni, Co, and V in olivines (Usui et al., 2008; Nakada et al., 2020) and thus is directly relevant to the results. The new results on this S-bearing martian melt composition, obtained at conditions of martian magma genesis, are then used to interpret trace metal contents in martian magmatic suites. The FRTE are very useful elements utilized in determining source characteristics and origin of planetary basalts, and evaluation of the role of S will make their prediction more accurate and applicable to natural systems such as martian magmas.

Experimental and analytical methods

Y-980459 is an olivine-phyric shergottite (martian meteorite) interpreted as representing a Martian primary mantle melt based on its bulk and olivine Mg#, Ni and Cr contents (Usui et al., 2008; Greshake et al. 2004), is ideal for this study, and experiments employed a synthesized Y-980459 composition (Shirai and Ebihara, 2004) for major and minor elements. Synthetic glass of the Y-980459 composition was prepared from reagent grade oxide powders in an agate mortar. This mixture was then fused into glass at fO_2 of ~FMQ buffer, and then reground into a powder followed by addition of ~200 ppm V, Co and Ni. This starting composition was then split into four aliquots; each of them was prepared to contain 0, 1000, 2000, and 3000 ppm S,

137 respectively, by the addition of pyrite (FeS_2) powder. The addition of minor amount of FeS_2 (up
138 to 3000 ppm) did not alter the phase relations of the run products.

139 Melting experiments were conducted using a Quickpress non-end-loaded piston-cylinder
140 apparatus at Johnson Space Center (JSC). Pressure was generated within $BaCO_3$ cells, and
141 calibrated on the location of the diopside-melting curve; pressures were corrected by –0.3 kbar
142 and only corrected pressures are reported [see Filiberto et al. (2008) for calibration results].
143 Experimental details of pressure, temperature and the assemblies were also presented in Righter
144 et al. (2009) and Filiberto et al. (2008). Samples were heated with graphite furnaces. A type C
145 thermocouple (W–Re) wire, with an accuracy of ±2 °C, was used to measure the temperature.
146 Samples were pressurized to the desired pressure (0.75 GPa), and then heated above the liquidus
147 temperature (1525 °C) for 0.5 hour before dropping to the target temperatures of 1450, 1475, and
148 1500 °C. The initial superheating followed by cooling to sub-liquidus temperatures is to
149 promote growth of large olivine crystals, as superheating should destroy more olivine nucleation
150 sites in the melt. Experiments were terminated by power quenching the samples, usually
151 resulting in glassy run products.

152 All major elements in olivines and glasses were analyzed with a Cameca SX100 electron
153 microprobe at NASA-JSC, using an accelerating voltage of 20 kV and sample current of 20 nA.
154 Standards included both natural (kaersutite, andradite, wollastonite, chromite, rutile, olivine,
155 rhodonite, potassium feldspar, albite) and synthetic (V metal, NiO) standard materials. Count
156 times for major elements were typically 10 s, and as long as 120 s for low concentrations of V or
157 Cr in olivines and glasses. Under the latter conditions, detection limits were approximately 100
158 ppm for V. Interference of Ti*K*α on V*K*α peaks (Snetsinger et al. 1968) were avoided by
159 counting Ti on PET using integral mode, and V on LiF in differential mode. PAP φ-ρ-Z

corrections were used in data reduction (Pouchou and Pichoir, 1991). All analyses are reported in **Tables 1 and 2**.

Ion microprobe analyses of experimental charges were conducted using a Cameca IMS 4f instrument at the University of New Mexico following the approach of Shearer et al. (1990, 2005, 2006) The olivine analyses involved repeated cycles of peak counting on $^{51}V^{+}$, $^{59}Co^{+}$, $^{60}Ni^{+}$, and $^{30}Si^{+}$. Ten cycles were used per analysis. The $^{30}Si^{+}$ was used as a reference species. The analytical procedure included counting on a background position to monitor detection noise. Background was collected on each standard and unknown at mass 18.7. Measurements at this mass produced a background of 1-3 counts. Absolute concentrations of each element were calculated using empirical relationships of measured peak $^{51,59,60}X^{+}/^{30}Si^{+}$ ratios normalized to known SiO_2 content (calibration curves are $((^{51,59,60}X^{+}/^{30}Si^{+}) \times SiO_2)$ plotted against trace elements for each standard) to element concentrations as derived from daily calibration measurements of the following olivine and glass standards: KAUG, K1OPX, D1OL, PM150, SC, MARJ, 610, 614, WUSTL1, and WUSTL2. Calibration curves for these elements have previously been determined by Papike et al.(1999) and Shearer et al. (1996, 2006). Analyses were made by bombardment of the sample with primary O^{-} ions accelerated through a nominal potential of 10 kV. A primary ion current of 15-20 nA was focused on the sample over a spot diameter of 15 µm. Sputtered secondary ions were energy filtered using a sample offset voltage of -105 V, and an energy window of ±25 V, to eliminate effectively most isobaric interferences (Shimizu et al., 1978). Secondary ions are detected by an electron multiplier in pulse counting mode. Peak counting times were varied to optimize precision. For olivine and glass analyses, precisions of better than 3% and 5%, respectively, were achieved. All ion microprobe analyses were conducted at locations analyzed previously with the electron microprobe, and the SiO_2

concentrations determined by EMP were used in reducing the SIMS data. Inclusion of contaminating phases in the SIMS analyses was avoided by selecting optically clean olivine grains and by mass imaging of major elements before and after each spot SIMS analysis.

Results

Phase equilibrium

Experimental charges mainly consist of olivine (Fo_{81-84}) and glass (**Figure 2**). Melt fractions were determined by using Ca mass balance between the bulk composition, glass and olivine, and varied from 0.85 to 0.98 in weight. Spinel is present only in two 1450 °C charges, the lowest temperature of our experimental suite. No sulfide phases are observed in the charges, suggesting sulfide under-saturation. Run products were sliced vertically to ensure that sulfide liquids had not settled to the bottom of the experimental charge. Neither olivines (typically >100 μm) nor glasses are zoned and are compositionally homogeneous in each experiment. The Fe-Mg exchange coefficient [K_d(Fe-Mg) = D(Fe)/D(Mg)] values between olivine and glass (0.28-0.36) suggest that the experiments closely approached equilibrium (e.g., Filiberto and Dasgupta, 2011).

Oxygen fugacity

Our graphite capsule does not buffer fO_2 in systems that contain melt – instead fO_2 is ultimately established in each experimental run by an interplay between Fe^{3+}/Fe^{2+}, CO_2 solubility and graphite-CO-CO_2 gas equilibria (Pawley et al., 1992; Holloway et al., 1992). Because every bulk composition has a slightly different CO_2 solubility, and different FeO and Fe_2O_3 content, these equilibria can define fO_2 across a window from FMQ-3 to FMQ, and thus it has to be measured for each specific bulk composition. Righter et al. (2009) and Righter et al (2013) used Co-(CoO,MgO) sliding sensor (after Taylor et al., 1992) for shergottite melt compositions to

calculate fO_2 for experiments in graphite capsules and they are FMQ-1.5. This relative fO_2 is slightly higher than measured in Y98 (FMQ-2.5 to FMQ-3.5; Shearer et al., 2006; Nakada et al., 2020), but the difference is not significant enough to influence partitioning and this will be discussed in more detail below.

Partition and exchange coefficients

Partition coefficients, D(M) olivine/melt, are the ratio of wt% element M in the olivine / wt% element M in silicate melt, and are known to vary with temperature, pressure, melt composition, and fO_2. Because D(M)'s can be dependent upon subtle melt compositional parameters, and temperature and oxygen fugacity, it is useful to also examine exchange coefficients based on the equilibria such as

$$MO + Mg_2SiO_4 = MgO + MgMSiO_4$$
melt olivine melt olivine

where M = V, Cr, Mn, Fe, Co or Ni, and the $K_d(M\text{-}Mg) = (X_{M2SiO4})(X_{MgO}) / (X_{MO})(X_{MgMSiO4})$ which simplifies to D(M)/D(Mg). We examine Ni, Co, Mn, V and Cr partitioning between olivine and melt using both the partition coefficient and exchange coefficients (**Table 3**), to examine the effect of S on partitioning of these elements.

The D(M) values for Ni, Co, show a slight decrease and those for V, Cr, and Mn exhibit no variation with increasing S contents (up to 3066 ppm). On the other hand, the ln K_d(M-Mg) values for all five elements decrease with increasing melt S contents (**Fig. 3a,b; Figure 4a,b**). Because partitioning is sometimes dependent upon melt composition or structure, we use the ratio of non-bridging oxygen to tetrahedrally coordinated cations (NBO/T), which is a gauge of melt structure using composition (Mysen, 1991). NBO/T is a simple concept of melt

polymerization that can be used to assess variation in melt composition from a polymerized melt like a rhyolite (NBO/T < 1) to more depolymerized like peridotitic melt (NBO/T=2.7). The D(M) values for Ni decrease slightly with increasing NBO/T, whereas those for Co, V, Cr, and Mn all show little to no correlations (**Fig. 3c,d**). On the other hand, $\ln K_d$(M-Mg) values for Ni, Mn, V, and Cr all increase with increasing NBO/T and those for Co remain nearly constant (**Fig. 4c,d)**. Examination of D(M) and $\ln K_d$(M-Mg) variation with NBO/T and Sulfur shows more correlations with NBO/T, and may indicate the importance of melt compositional effects for olivine/melt partitioning of Ni, Co, Mn, V, and Cr. Trends with melt S content and melt composition and/or structure (NBO/T) might be inter-related or co-dependent and so below we look at previous studies for guidance on how to interpret our results.

Discussion

Comparison to previous studies

There have been many systematic studies of trace metal partitioning that can be compared to our new results. When making comparisons, differences in temperature, fO_2, and melt composition are important to understand. For example, Mallmann and O'Neill (2013) studied V, Mn, and Cr between 1200 and 1530 °C, FMQ-2.85 to +3, with melts including a wide range of FeO contents, but higher Al_2O_3 contents than martian melts, and no sulfur. LeRoux et al. (2011) studied Ni, Co, and Mn at 1310-1500 °C, FMQ-1.5, and for terrestrial basaltic melts with low FeO, high Al_2O_3, and no S. Gaetani and Grove (1997) carried out experiments at 1350 °C, FMQ-1 to -4, on terrestrial basaltic melt compositions with high Al_2O_3, and low FeO. Their study had variable melt S contents up to ~ 1500 ppm, and also a specified f_{S2}. Filiberto et al.

(2009) examined Ni partitioning at 1300-1420 °C, FMQ-2, for an S-free Gusev (Martian) basalt melt composition. Herd et al. (2009) studied Ni and Co between 1150 and 1290 °C, FMQ-0.5 to -3.0, for three S-free melt compositions (martian, lunar, eucritic). Matzen et al. (2013) studied Ni between 1350 and 1500 °C, 1 bar to 3 GPa, FMQ-1.7, for melts of mid-ocean ridge basalt composition. Hanson and Jones (1998) examined Cr partitioning between olivine and melt for various melt compositions, 1160-1230 °C, and at FMQ and FMQ-4. With a goal of evaluating Ni and Co behavior at high temperatures relevant to a lunar magma ocean, Longhi et al. (2010) studied olivine/melt partitioning to over 2000 °C and FMQ-4. Shearer et al. (2006) studied V at 1300-1380 °C, FMQ to FMQ-4.5, and for S-free Yamato 980459 melt compositions. Elardo et al. (2011) measured Ni and Co partitioning in two lunar mantle bulk compositions and at near liquidus conditions between 1 and 3 GPa, and up to 1800 C. Tuff et al. (2010) studied Ni, Co, V, Cr, Mn at 1370-1400 °C, with melts that were medium in FeO and Al_2O_3, FMQ-2 to -3, and variable S. Given the overlap in elements, S-contents and fO_2, their study will be of interest to compare directly to our results. These experiments will be very useful for making comparison of V, Cr, and Mn results at the same T, fO_2, and melt FeO.

Effect of temperature with D(Mg) as a proxy

Previous work has shown that D(Mg) olivine/melt is a good proxy for temperature dependence of partitioning (Jones, 2003, 1995, 1984; Matzen et al., 2013). This is demonstrated with numerous studies for all five elements (**Figure 5**). Positive correlations of D(M) and D(Mg) are observed for Ni, Co, Mn and Cr. Correlations with D(V) are not as clear, but this is due to the strong dependence of D(V) on fO_2 (see next section).

Effect of oxygen fugacity

There is no clear dependence of D(Ni), D(Co), or D(Mn) on oxygen fugacity as might be expected for these three elements that exhibit 2+ valence in fO_2 range of natural magmas. Chromium exhibits two oxidation states in natural magma – 2+ and 3+, yet D(Cr) does not exhibit strong dependence upon fO_2, as the Cr^{2+}/Cr (tot) varies only slightly across the fO_2 range of natural magmas (Hanson and Jones, 1998; Bell et al., 2017). However, D(V) varies strongly with fO_2 (**Figure 5**), and strong fO_2 dependence has led some previous studies to utilize D(V) olivine/melt as an oxybarometer (Hanson and Jones, 1997; Canil and Fedortchouk, 2001; Mallmann and O'Neill, 2013). When our study is combined with several literature datasets, D(V) clearly varies between 0.001 and 0.4 between FMQ+3 and FMQ-3 (**Figure 5**). The decrease in D(V) at higher fO_2 is caused by a shift from lower valence of V (3+ and 2+) at lower fO_2 to higher valence of V (4 and 3+) at higher fO_2 (e.g., Sutton et al., 2005; Righter et al., 2006).

Effect of melt composition

Melt composition is considered an important variable for Ni, Co, and V partitioning between olivine and melt (Herd et al., 2009; Filiberto et al., 2009; Mallmann and O'Neill, 2013; Tuff and O'Neill, 2010; Matzen et al., 2013). Because of the potential for melt compositional effects, we use the NBO/T melt compositional/structural parameter to assess the effects for each element. D(M) exhibits clear dependence on NBO/T for all five elements (**Figure 5**). For our experiments, K_d(M-Mg) values are also correlated with melt compositions (**Figure 3c, d and 4c, d**). For example, K_d(Ni-Mg), K_d(V-Mg), K_d(Cr-Mg), and K_d(Mn-Mg) all increase with increasing NBO/T in the silicate melts (**Fig. 4c, 4d, 6)**. In contrast, K_d(Co-Mg) is nearly constant among the samples in our experimental series, (**Fig. 4c, 6**). Thus, predictive expressions for all

of these elements will have to include terms for D(Mg), fO_2, and melt composition, and are developed in more detail below with specific studies forming the foundation for comparison.

Effect of S on olivine/melt partition coefficients

To assess the independent contribution of S on the siderophile element partitioning between olivine and melt, we calculate D(M) utilizing predictive expressions whose specific form is based on our assessment in the previous section.

Because we are searching for variations in D(Ni) or D(Co) well outside of the experimental error associated with these predictive expressions (typically 10-15%), we will use a simple form to predict D(Ni) and D(Co) in S-free systems to compare to our S-bearing experiments, using D(Mg) and NBO/T as the independent variables. Because Mn does not exhibit valence change across the fO_2 range considered relevant to terrestrial, martian or lunar samples utilized in these studies, and thus it should exhibit similar behavior to Ni and Co, we use these correlations with D(Mg) for Mn as well. Thus, for Ni, Co, and Mn we use D(Ni) = a D(Mg) + b (NBO/T) + d, calibrated with S-free experiments that were carried out at otherwise similar conditions (Ni and Co: Longhi et al., 2010; LeRoux et al., 2011; Tuff and O'Neill, 2010; Herd et al., 2009; Filiberto et al., 2009; Elardo et al., 2011; Mn: Tuff and O'Neill, 2010; Mallmann and O'Neill, 2013; LeRoux et al., 2011; and Longhi et al.,2010). Previous studies have adequately modelled D(Ni) and D(Co) as a function of D(Mg) (Jones, 1995; Matzen et al., 2014; Herd et al., 2009).

V and Cr both show dependence upon D(Mg) and NBO/T like Ni, Co, and Mn. In addition, studies have shown that D(V) is dependent upon melt composition (Mallmann and O'Neill, 2013). Since these two elements exhibit valence changes over the oxygen fugacities of

316 relevance to terrestrial, martian or lunar samples utilized in these studies, D(V) and D(Cr) will
317 vary with fO_2. Thus, for V and Cr, we use the expression D(V) = a D(Mg) + b (NBO/T) + c
318 (ΔFMQ) + d, calibrated with data from Mallmann and O'Neill (2013), Tuff and O'Neill (2010),
319 and Elardo et al. (201) (For V) and data from experiments of Tuff and O'Neill (2010),
320 Mallmann and O'Neill (2013), Longhi et al. (2010), and Hanson and Jones (1998) (for Cr),
321 across a wide T, fO_2 and melt composition range.

322 Multiple linear regression of D(M) against the two or three variables was done using
323 Sigma Plot 12. Regression results are summarized in **Table 4**, and **Figure 7**. The data used to
324 derive the regression coefficients cover a wide range of temperature, melt composition and fO_2.
325 The standard error associated with each equation is small, and this error will be critical to
326 evaluating and isolating the effect of sulfur on the olivine/melt partitioning of each element. The
327 difference between the predicted values to the measured values for each of our experiments
328 (**Figure 8**) shows that for most or all of the range of sulfur content, the measured values is within
329 error the same as the predicted value, thus indicating that sulfur does not have a strong effect on
330 partitioning for most elements. However, Co exhibits statistically different values at the highest
331 S contents, indicating that D(Co) can be lower in S-bearing systems compared to S-free. Thus,
332 at the highest S melt values explored here, D(Co) will be slightly lowered, but all other elements
333 – Ni, Mn, Cr, and V – show no variation outside the predicted values in S-free systems.

334 Although our experimental studies suggest that S could slightly reduce partition
335 coefficients of siderophile elements, both D(Ni) and D(Co) are still distinctly greater than one
336 even in our highest S (~3000 ppm) melts. Whether Co can become incompatible depends on
337 how much sulfur is dissolved into the melt, at what temperature, and whether the melts are
338 sulfide saturated. There is evidence from both bulk S and highly siderophile elements that

martian melts are sulfide under-saturated (Jones et al., 2003; Righter et al., 2009). However, putting this data aside for a moment, we calculate S content at sulfide saturation to illustrate the potential effect on D(Co) olivine/melt of the highest possible melt S contents. For example, if shergottitic liquids are sulfide saturated in their mantle source, contain >4000 ppm S, and liquidus olivines crystallize at a temperature of ~1450-1500 C, these conditions could push D(Co) to values near or below 1. To test under what conditions D(Co) becomes <1, we have added our S-bearing dataset, as well as S-bearing experiments from Gaetani and Grove (1997) and Tuff and O'Neill (2010), to the regression analysis, and a sulfur term to quantify the effect of dissolved S on D(Co). The equation has the form: D(Co) = a D(Mg) + b(NBO/T) + d (ppm S) + e, and results in a = 0.495 , b = -0.311, d = -0.0000824, e = 0.843, with standard error = 0.22 (**Table 4**). Application of this equation to martian primary liquids (NBO/T = 1.5, D(Mg) = 2.5) results in D(Co) < 1 if S contents are >8000 ppm. These values are a factor of ~4 higher than measured in primitive martian basalts (1600-2700 ppm S; Ding et al., 2015; Righter et al., 2009 and references within), and are 2 times higher than S contents expected if such melts were sulfide saturated in their source (~ 4000 ppm). Therefore, dissolved sulfur is not a realistic way to lower D(Co), even under high S, sulfide saturated conditions.

Conclusions and implications

This investigation demonstrates that dissolved S in melts has minimal to no effect on the olivine/melt partitioning of Ni, Co, Mn, V and Cr. Only at high S contents of ~3000 ppm or higher is there a discernable difference in partitioning for Co. These results are essentially consistent with Tuff and O'Neill (2010) whose results suggest that S in the silicate melt has a barely discernible effect on Fe, Co and Ni partition coefficients. Furthermore, they did not

recognize detectable effects on Cr, Mn and V. Considering S solubility for primitive martian melts (such as Y-980459) can be as high as ~4000 ppm within a range of reasonable shergottite magmatic conditions (Righter et al., 2009), the olivine/melt partition coefficients for these five elements will only be affected at near sulfide saturation conditions; S contents in sulfide-under-saturated martian liquids are typically not high enough (~1500-2000 ppm) to affect the partitioning.

If a change in olivine/melt compatibility is not responsible for the Ni and Co systematics in shergottite olivine, another mechanism or process is causing the apparent incompatibility of Co in shergottite olivines. The de-coupling of Ni and Co is also observed in lunar and terrestrial igneous suites (Sobolev et al., 2007; Karner et al., 2003; Papike et al., 1999), suggesting that finding a solution to the martian sample suite might have wider implications for planetary basalts. Lower oxygen fugacity cannot be an explanation because studies have shown that neither D(Ni) nor D(Co) olivine/melt are dependent upon fO_2 (e.g., **Figure 5**). High temperatures can cause lowering of D(Ni) and D(Co), but even as Longhi et al. (2010) show, the temperatures required are ~ 2000 °C, which are superliquidus for the shergottite or primary martian mantle melts. Changes during fractionation might be called upon to affect the behavior of Co relative to Ni, but the partitioning of these elements would be controlled by clinopyroxene and spinel as other magmatic phases, both of which are hosts for Ni and Co and thus exhibit compatible behavior as well (Righter et al., 2006; Dygert et al., 2014). An additional possible mechanism is a difference in diffusion behavior between Co and Ni in olivine at these conditions. There is diffusion data for both elements that indicates they have very similar diffusion coefficients (Morioka, 1980; 1981), so a diffusion-controlled mechanism is unrealistic

as well. Thus, changes in Ni or Co behavior due to fO_2, temperature, fractionation, or diffusion are not viable explanations.

One possibility, suggested by Herd et al. (2009), is that magma mixing may have altered the concentrations of Ni and Co, leading to the apparent incompatible behavior. Shearer et al. (2013) and Usui et al. (2008) suggested the possibility that Y98 olivine cores are xenocrystic. This idea is supported by the presence of xenocrysts in many of the olivine-phyric shergottites (e.g., Castle et al., 2020). Another possibility would require assimilation of a Co-rich material into the shergottite primary liquids after the initial crystallization of olivine, thus causing an apparent incompatibility of Co. Such Co-rich material on Mars is apparently not common, but has been identified in exploration of the Gale Crater region of Mars (Lanza et al., 2016; Berger et al., 2017). Co-rich (~300 ppm Co) and Mn-rich (~3.5 wt.%) deposits have been documented there, associated with hydrothermal activity and oxidation, and the possible presence of oxides. The positive correlation of Co and Mn in olivines and bulk shergottites (and negative correlation with Ni) might support such an idea. A third possibility is that the Ni and Co trends documented in the shergottite olivines are due to possible kinetic crystallization effects (e.g., Kennedy et al., 1993; Papike et al., 1999; Hagerty et al., 2006; Albarede and Bottinga, 1972). All three of these possibilities could be fruitful avenues for future investigations.

Implications

Our partitioning results, in combination with previously published data, show that dissolved sulfur does not affect olivine/melt partitioning of Ni, Mn, Cr, or V, but might have a small effect on Co. However, nearly 8000 ppm of sulfur would be required in martian primary melts for Co to become incompatible ($D(Co) < 1$), 2 times higher than those of a sulfide saturated melt at the (P,T) conditions of a martian mantle source region. Therefore, the anomalous

incompatible behavior observed in these primary magma suites must be due to another mechanism. High temperature, oxygen fugacity, and diffusion are not viable mechanisms, but magma mixing, assimilation, or kinetic crystallization effects remain possibilities.

Acknowledgements

This research was supported by an RTOP to KR from Mars Fundamental Research program, and support from the NASA Planetary Science Directorate (KR), the NASA Postdoctoral Program (TU), Emerging Worlds and Mars Fundamental Research programs (CKS) and the Lunar and Planetary Institute (CKS). We are indebted to Loan Le and Anne Peslier for their technical expertise and assistance in the experimental and analytical laboratories, respectively. We are also grateful for the reviews of V. le Roux and an anonymous reviewer for their helpful constructive comments.

References:

Albarede, F. and Bottinga, Y. (1972) Kinetic disequilibrium in trace element partitioning between phenocrysts and host lava. Geochimica et Cosmochimica Acta 36, 141-156.

Beattie, P., Ford, C., and Russell, D. (1991) Partition coefficients for olivine-melt and orthopyroxene-melt systems. Contributions to Mineralogy and Petrology 109, 212-224.

Bell, A.S., Shearer, C., Burger, P., Ren, M., Newville, M., and Lanzirotti, A. (2017) Quantifying and correcting the effects of anisotropy in XANES measurements of chromium valence in olivine: Implications for a new olivine oxybarometer. American Mineralogist 102, 1165-1172.

428 Berger, J.A., Schmidt, M.E., Gellert, R., Boyd, N.I., Desouza, E.D., Flemming, R.L., Izawa,
429 M.R., Ming, D.W., Perrett, G.M., Rampe, E.B., and Thompson, L.M. (2017) Zinc and
430 germanium in the sedimentary rocks of Gale Crater on Mars indicate hydrothermal
431 enrichment followed by diagenetic fractionation. Journal of Geophysical Research:
432 Planets 122, 1747-1772.

433 Canil, D. and Fedortchouk, Y. (2001) Olivine–liquid partitioning of vanadium and other trace
434 elements, with applications to modern and ancient picrites. The Canadian Mineralogist 39,
435 319-330.

436 Castle, N., Kuehl, E., Jones, J., and Treiman, A. (2020) Multiple origins of xenoliths and
437 xenocrysts in the Elephant Moraine 79001 Lithology A olivine-phyric
438 shergottite. Meteoritics & Planetary Science 55, 3-19.

439 Collinet, M., Médard, E., Charlier, B., Vander Auwera, J., and Grove, T.L. (2015) Melting of the
440 primitive Martian mantle at 0.5–2.2 GPa and the origin of basalts and alkaline rocks on
441 Mars. Earth and Planetary Science Letters 427, 83-94.

442 Ding, S., Dasgupta, R., Lee, C.T.A. and Wadhwa, M. (2015) New bulk sulfur measurements of
443 Martian meteorites and modeling the fate of sulfur during melting and crystallization–
444 Implications for sulfur transfer from Martian mantle to crust–atmosphere system. Earth and
445 Planetary Science Letters 409, 157-167.

446 Dreibus, G., Palme, H., Rammensee, W., Spettel, B., Weckwerth, G., and Wänke, H. (1982)
447 Composition of shergotty parent body: Further evidence for a two component model of
448 planet formation. Lunar and Planetary Science Conference XIII, 186-187.

449 Dreibus, G., Spettel, B., Haubold, R., Jochum, K.P., Palme, H., Wolf, D., and Zipfel, J. (2000)
450 Chemistry of a new shergottite: Sayh al Uhaymir 005. Meteoritics and Planetary Science
451 Supplement, 35, A49.

452 Dygert, N., Liang, Y., Sun, C., and Hess, P. (2014) An experimental study of trace element
453 partitioning between augite and Fe-rich basalts. Geochimica et Cosmochimica Acta 132,
454 170-186.

455 Elardo, S.M., Draper, D.S., and Shearer Jr, C.K. (2011) Lunar Magma Ocean crystallization
456 revisited: Bulk composition, early cumulate mineralogy, and the source regions of the
457 highlands Mg-suite. Geochimica et Cosmochimica Acta 75, 3024-3045.

458 Filiberto, J. and Dasgupta, R. (2011) Fe^{2+}–Mg partitioning between olivine and basaltic melts:
459 Applications to genesis of olivine-phyric shergottites and conditions of melting in the
460 Martian interior. Earth and Planetary Science Letters 304, 527-537.

461 Filiberto, J., Treiman, A.H., and Le, L. (2008) Crystallization experiments on a Gusev
462 Adirondack basalt composition. Meteoritics & Planetary Science 43, 1137-1146.

463 Filiberto, J., Jackson, C., Le, L., and Treiman, A.H. (2009) Partitioning of Ni between olivine
464 and an iron-rich basalt: Experiments, partition models, and planetary implications. American
465 Mineralogist 94, 256-261.

466 Filiberto J., Musselwhite D., Gross J., Burgess K., Le L., and Treiman A.H. (2010) Experimental
467 petrology, crystallization history and parental magma characteristics of olivine - phyric
468 shergottite NWA 1068: Implications for the petrogenesis of “enriched” olivine - phyric
469 shergotites. Meteoritics & Planetary Science 45, 1258–1270.

Franz, H.B., Kim, S.T., Farquhar, J., Day, J.M., Economos, R.C., McKeegan, K.D., Schmitt, A.K., Irving, A.J., Hoek, J. and Dottin III, J. (2014) Isotopic links between atmospheric chemistry and the deep sulphur cycle on Mars. Nature 508, 364-368.

Gaetani, G.A. and Grove, T.L. (1997) Partitioning of moderately siderophile elements among olivine, silicate melt, and sulfide melt: Constraints on core formation in the Earth and Mars. Geochimica et Cosmochimica Acta 61, 1829-1846.

Goodrich, C.A. and Delaney, J.S. (2000) Fe/Mg–Fe/Mn relations of meteorites and primary heterogeneity of primitive achondrite parent bodies. Geochimica et Cosmochimica Acta 64, 149-160.

Greshake, A., Fritz, J., and Stöffler, D. (2004) Petrology and shock metamorphism of the olivine-phyric shergottite Yamato 980459: Evidence for a two-stage cooling and a single-stage ejection history. Geochimica et Cosmochimica Acta 68, 2359-2377.

Gross J., Treiman A.H., Filiberto J., and Herd C.D.K. (2011) Primitive olivine - phyric shergottite NWA 5789: Petrography, mineral chemistry, and cooling history imply a magma similar to Yamato - 980459. Meteoritics & Planetary Science 46, 116–133.

Hagerty, J.J., Shearer, C.K., Vaniman, D.T., and Burger, P.V. (2006) Identifying the effects of petrologic processes in a closed basaltic system using trace-element concentrations in olivines and glasses: Implications for comparative planetology. American Mineralogist 91, 1499-1508.

Hanson, B. and Jones, J.H. (1997) The contrasting partitioning behavior of V and Cr into olivine. Eos Transactions AGU **78,** 335.

491 Hanson, B. and Jones, J.H. (1998) The systematics of Cr^{3+} and Cr^{2+} partitioning between olivine
492 and liquid in the presence of spinel. American Mineralogist 83, 669-684.

493 Herd, C.D., Dwarzski, R.E., and Shearer, C.K. (2009) The behavior of Co and Ni in olivine in
494 planetary basalts: An experimental investigation. American Mineralogist 94, 244-255.

495 Herzberg, C., Vidito, C., and Starkey, N.A. (2016) Nickel–cobalt contents of olivine record
496 origins of mantle peridotite and related rocks. American Mineralogist 101, 1952-1966.

497 Holloway, J.R., Pan, V., and Gudmundsson, G. (1992) High-pressure fluid-absent melting
498 experiments in the presence of graphite: oxygen fugacity, ferric/ferrous ratio and dissolved
499 CO_2. European Journal of Mineralogy 4, 105-114.

500 Holzheid, A. and Grove, T. L. (2002) Sulfur saturation limits in silicate melts and their
501 implications for core formation scenarios for terrestrial planets. American Mineralogist 87,
502 227-237.

503 Humayun, M., Qin, L., and Norman, M.D. (2004) Geochemical evidence for excess iron in
504 the mantle beneath Hawaii. Science 306, 91-94.

505 Jones, J.H. (1984) Temperature- and pressure-independent correlations of olivine/liquid
506 partition coefficients and their application to trace element partitioning. Contributions
507 to Mineralogy and Petrology 88, 126-132.

508 Jones, J.H. (1995) Experimental trace element partitioning. In T.J. Ahrens, Ed., Rock Physics &
509 Phase Relations: A Hand Book of Physical Constants, p. 73-104, American Geophysical
510 Union, Washington, DC.

511 Jones, J.H. (2003) A liquidus geothermometer for SNC, lunar, and eucritic magmas. Lunar and
512 Planetary Science XXXIV, Abstract #1130.

513 Jones, J.H., Neal, C.R., and Ely, J.C. (2003) Signatures of the highly siderophile elements in the
514 SNC meteorites and Mars: a review and petrologic synthesis. Chemical Geology 196, 5-25.

515 Karner, J., Papike, J.J., and Shearer, C.K. (2003) Olivine from planetary basalts: Chemical
516 signatures that indicate planetary parentage and those that record igneous setting and
517 process. American Mineralogist 88, 806-816.

518 Kennedy, A.K., Lofgren, G.E., and Wasserburg, G.J. (1993) An experimental study of trace
519 element partitioning between olivine, orthopyroxene and melt in chondrules: equilibrium
520 values and kinetic effects. Earth and Planetary Science Letters 115, 177-195.

521 Lanza, N.L., Wiens, R.C., Arvidson, R.E., Clark, B.C., Fischer, W.W., Gellert, R., ... and Rice,
522 M. S. (2016) Oxidation of manganese in an ancient aquifer, Kimberley formation, Gale
523 crater, Mars. Geophysical Research Letters 43, 7398-7407.

524 Laurenz, V., Fonseca, R.O., Ballhaus, C., Jochum, K.P., Heuser, A., and Sylvester, P.J. (2013)
525 The solubility of palladium and ruthenium in picritic melts: 2. The effect of
526 sulfur. Geochimica et Cosmochimica Acta 108, 172-183.

527 Lee, C.T.A., Brandon, A.D., and Norman, M. (2003) Vanadium in peridotites as a proxy for
528 paleo-fO_2 during partial melting: prospects, limitations, and implications. Geochimica et
529 Cosmochimica Acta 67, 3045-3064.

Le Roux, V., Dasgupta, R., and Lee, C.T. (2011) Mineralogical heterogeneities in the Earth's mantle: constraints from Mn, Co, Ni and Zn partitioning during partial melting. Earth and Planetary Science Letters 307, 395-408.

Le Voyer, M., Hauri, E.H., Cottrell, E., Kelley, K.A., Salters, V.J., Langmuir, C.H., Hilton, D.R., Barry, P.H. and Füri, E. (2019) Carbon Fluxes and Primary Magma CO_2 Contents Along the Global Mid - Ocean Ridge System. Geochemistry, Geophysics, Geosystems 20, 1387-1424.

Li, C., Ripley, E.M., and Mathez, E.A. (2003) The effect of S on the partitioning of Ni between olivine and silicate melt in MORB. Chemical Geology 201, 295-306.

Libourel, G. (1999) Systematics of calcium partitioning between olivine and silicate melt: implications for melt structure and calcium content of magmatic olivines. Contributions to Mineralogy and Petrology 136, 63-80.

Longhi, J., Durand, S.R., and Walker, D. (2010) The pattern of Ni and Co abundances in lunar olivines. Geochimica et Cosmochimica Acta 74, 784-798.

Mallmann, G. and O'Neill, H.St.C. (2013) Calibration of an empirical thermometer and oxybarometer based on the partitioning of Sc, Y and V between olivine and silicate melt. Journal of Petrology 54, 933-949.

Matzen, A.K., Baker, M.B., Beckett, J.R. and Stolper, E.M. (2013) The temperature and pressure dependence of nickel partitioning between olivine and silicate melt. Journal of Petrology 54, 2521-2545.

Morioka, M. (1980) Cation diffusion in olivine—I. Cobalt and magnesium. Geochimica et Cosmochimica Acta 44, 759-762.

551 Morioka, M. (1981) Cation diffusion in olivine—II. Ni-Mg, Mn-Mg, Mg and Ca. Geochimica et
552 Cosmochimica Acta 45 1573-1580.

553 Mysen, B.O. (1991) Relations between structure, redox equilibria of iron, and properties of
554 magmatic liquids. In L.L. Perchuk, Ed., Physical Chemistry of Magmas, p. 41-98, Springer,
555 New York, NY.

556 Nakada, R., Usui, T., Ushioda, M., and Takahashi Y. (2020) Vanadium micro-XANES
557 determination of oxygen fugacity in olivine-hosted glass inclusion and groundmass glasses of
558 martian primitive basalt Yamato 980459. American Mineralogist 105, 1695-1703.

559 Papike, J.J. (1998) Comparative Planetary Mineralogy: Chemistry of Melt- Derived Pyroxene,
560 Feldspar, and Olivine. In J.J. Papike, Ed., Planetary Materials, 36, 7-01 - 7-12. Reviews in
561 Mineralogy and Geochemistry, Mineralogical Society of America, Chantilly, Virginia.

562 Papike, J.J., Fowler, G.W., Adcock, C.T., and Shearer, C.K. (1999) Systematics of Ni and Co in
563 olivine from planetary melt systems: Lunar mare basalts. American Mineralogist 84, 392-
564 399.

565 Papike, J.J., Karner, J.M., Shearer, C.K., and Burger, P.V. (2009) Silicate mineralogy of martian
566 meteorites. Geochimica et Cosmochimica Acta 73, 7443-7485.

567 Pawley, A.R., Holloway, J.R., and McMillan, P.F. (1992) The effect of oxygen fugacity on the
568 solubility of carbon-oxygen fluids in basaltic melt. Earth and Planetary Science Letters 110,
569 213-225.

570 Pouchou, J.L. and Pichoir, F. (1991) Quantitative analysis of homogeneous or stratified
571 microvolumes applying the model “PAP”. In K.GF.J. Heinrich and D. Newbury, Eds.,
572 Electron Probe Quantitation, p. 31-75, Springer, Boston, MA.

573 Rapp, J. F., Draper, D. S., and Mercer, C. M. (2013) Anhydrous liquid line of descent of
574 Yamato - 980459 and evolution of Martian parental magmas. Meteoritics & Planetary
575 Science 48, 1780-1799.

576 Righter, K., Leeman, W.P., and Hervig, R.L. (2006) Partitioning of Ni, Co and V between
577 spinel-structured oxides and silicate melts: Importance of spinel composition. Chemical
578 Geology 227, 1-25.

579 Righter, K., Pando, K., and Danielson, L.R. (2009) Experimental evidence for sulfur-rich
580 martian magmas: Implications for volcanism and surficial sulfur sources. Earth and Planetary
581 Science Letters 288, 235-243.

582 Righter, K., Danielson, L.R., Pando, K., Morris, R.V., Graff, T.G., Agresti, D.G., Martin, A.M.,
583 Sutton, S.R., Newville, M., and Lanzirotti, A. (2013) Redox systematics of martian magmas
584 with implications for magnetite stability. American Mineralogist 98, 616-628.

585 Sato, H. (1977) Nickel content of basaltic magmas: identification of primary magmas and a
586 measure of the degree of olivine fractionation. Lithos 10, 113-120.

587 Shirai, N. and Ebihara, M. (2004) Chemical characteristics of a Martian meteorite, Yamato
588 980459. Antarctic Meteorite Research 17, 55-67.

589 Shearer, C.K. and Papike, J.J. (2005) Early crustal building processes on the moon: Models for
590 the petrogenesis of the magnesian suite. Geochimica et Cosmochimica Acta 69, 3445-3461.

591 Shearer, C.K., Papike, J.J., Simon, S.B., Shimizu, N., Yurimoto, H., and Sueno, S. (1990) Ion
592 microprobe studies of trace elements in Apollo 14 volcanic glass beads: Comparisons to
593 Apollo 14 mare basalts and petrogenesis of picritic magmas. Geochimica et Cosmochimica
594 Acta 54, 851-867.

595 Shearer, C. K., Papike, J. J., & Layne, G. D. (1996) Deciphering basaltic magmatism on the
596 Moon from the compositional variations in the Apollo 15 very low-Ti picritic magmas.
597 Geochimica et Cosmochimica Acta 60, 509-528.

598 Shearer, C.K., McKay, G.A, Papike, J.J., and Karner, J.M. (2006) Valence state partitioning of
599 vanadium between olivine-liquid: Estimates of the oxygen fugacity of Y980459 and
600 application to other olivine-phyric martian basalts. American Mineralogist 91, 1657-1663.

601 Shearer, C.K., Aaron, P.M., Burger, P.V., Guan, Y., Bell, A.S., and Papike, J.J. (2013)
602 Petrogenetic linkages among fO_2, isotopic enrichments-depletions and crystallization history
603 in Martian basalts. Evidence from the distribution of phosphorus in olivine megacrysts.
604 Geochimica et Cosmochimica Acta 120, 17-38.

605 Snetsinger, K.G., Bunch, T.E., and Keil, K. (1968) Electron microprobe analysis of vanadium in
606 the presence of titanium. American Mineralogist: Journal of Earth and Planetary
607 Materials 53, 1770-1773.

608 Sobolev, A.V., Hofmann, A.W., Kuzmin, D.V., Yaxley, G.M., Arndt, N.T., Chung, S.L.,
609 Danyushevsky, L.V., Elliott, T., Frey, F.A., Garcia, M.O. and Gurenko, A.A. (2007) The
610 amount of recycled crust in sources of mantle-derived melts. Science 316, 412-417.

611 Takahashi, E. (1978) Partitioning of Ni^{2+}, Co^{2+}, Fe^{2+}, Mn^{2+} and Mg^{2+} between olivine and
612 silicate melts: compositional dependence of partition coefficient. Geochimica et
613 Cosmochimica Acta 42, 1829-1844.

614 Taylor, J.R., Wall, V.J., and Pownceby, M.I. (1992) The calibration and application of accurate
615 redox sensors. American Mineralogist 77, 284-295.

616 Toplis, M.J. (2005) The thermodynamics of iron and magnesium partitioning between olivine
617 and liquid: criteria for assessing and predicting equilibrium in natural and experimental
618 systems. Contributions to Mineralogy and Petrology 149, 22-39.

619 Tuff, J. and O'Neill, H.St.C. (2010) The effect of sulfur on the partitioning of Ni and other first-
620 row transition elements between olivine and silicate melt. Geochimica et Cosmochimica
621 Acta 74, 6180-6205.

622 Usui, T., McSween Jr, H.Y., and Floss, C. (2008) Petrogenesis of olivine-phyric shergottite
623 Yamato 980459, revisited. Geochimica et Cosmochimica Acta 72, 1711-1730.

624 Wänke, H. and Dreibus, G. (1986) Geochemical evidence for the formation of the Moon by
625 impact-induced fission of the proto-Earth. In W. K. Hartmann, R. J. Phillips, and G. J.
626 Taylor, Eds., Origin of the Moon, p. 649-672, Lunar and Planetary Institute, Houston, TX.

627 Zipfel, J., Scherer, P., Spettel, B., Dreibus, G., and Schultz, L. (2000) Petrology and chemistry of
628 the new shergottite Dar al Gani 476. Meteoritics & Planetary Science 35, 95-106.

629

630

Figure Captions

Figure 1: Ni and Co concentrations in shergottite olivines showing compatible behavior of Ni with fractionation (or increasing XFe), and incompatible behavior of Co (from Papike et al., 2009; Shearer et al., 2008; Usui et al., 2008). These trends suggest that in shergottite systems Co exhibits incompatibility in olivine, counter to evidence from many partitioning studies that show it is compatible. Usui et al. (2008) also demonstrate Ni and Co incompatibility in high Fo olivines from Y-980459. Error on Ni and Co measurements are smaller than the symbols; arrows also show the direction of differentiation.

Figure 2: Back scattered electron image of run product from experiment #16, at 0.75 GPa, 1475 °C, with sample composition of synthetic Y-980459 melt with 1000 ppm S added. Duration was 3 hours, with a 30 minute dwell at 1500 °C before lowering to 1475 °C for olivine growth.

Figure 3: (a,b): D(M) versus S content [S] of coexisting melt for the experiments in this study. (a) Ni and Co, and (b) Mn, Cr, and V. Hatched line indicates a 1-sigma deviation of each regression line.

$D(Ni) = -0.0003 * [S] + 7.2739$ ($R^2 = 0.0365$);

$D(Co) = -(7x10^{-6}) * [S] + 1.4543$ ($R^2 = 0.0012$);

$D(Mn) = -(4x10^{-6}) * [S] + 0.7313$ ($R^2 = 0.0084$);

$D(Cr) = -(5x10^{-6}) * [S] + 0.5975$ ($R^2 = 0.0483$);

$D(V) = -(4x10^{-6}) * [S] + 0.2243$ ($R^2 = 0.0855$).

(c,d): D(M) versus NBO/T of coexisting melt for the experiments in this study; (c) Ni and Co, and (d) Mn, Cr, and V. Hatched line indicates a 1-sigma deviation of each regression line.

652 $D(Ni) = -1.6595 * (NBO/T) + 9.3734$ ($R^2 = 0.036$);

653 $D(Co) = -0.7374 * (NBO/T) + 2.532$ ($R^2 = 0.4018$);

654 $D(Mn) = -0.0857 * (NBO/T) + 0.8623$ ($R^2 = 0.1128$);

655 $D(Cr) = -0.0394 * (NBO/T) + 0.6497$ ($R^2 = 0.0917$);

656 $D(V) = + 0.0587 * (NBO/T) + 0.133$ ($R^2 = 0.548$).

657 **Figure 4: (a,b):** $\ln K_d$(M-Mg) versus S content [S] of coexisting melt for the experiments in this
658 study, where M = (a) Ni and Co, and (b) Cr and V. Hatched line indicates a 1-sigma deviation of
659 each regression line.

660 $\ln K_d(Ni\text{-}Mg) = -(1.11 \times 10^{-4}) * [S] + 0.970$ ($R^2 = 0.28$);

661 $\ln K_d(Co\text{-}Mg) = -(4.22 \times 10^{-5}) * [S] - 0.398$ ($R^2 = 0.282$);

662 $\ln K_d(Mn\text{-}Mg) = -(6.0 \times 10^{-5}) * [S] - 1.3162$ ($R^2 = 0.4057$);

663 $\ln K_d(Cr\text{-}Mg) = -(7.58 \times 10^{-5}) * [S] - 1.52$ ($R^2 = 0.468$);

664 $\ln K_d(V\text{-}Mg)$: $y = -(8.35 \times 10^{-5}) * [S] - 2.50$ ($R^2 = 0.299$).

665 **(c, d):** $\ln K_d$(M-Mg) versus NBO/T of coexisting melt for the experiments in this study, where M
666 = (c) Ni and Co, and (d) Mn, Cr, and V. Note that the S-rich melts have a lower NBO/T value
667 than S-poor melts. Hatched line indicates a 1-sigma deviation of each regression line.

668 $\ln K_d(Ni\text{-}Mg) = 0.4133 * NBO/T + 0.2211$ ($R^2 = 0.1027$);

669 $\ln K_d(Co\text{-}Mg) = 0.016 * NBO/T - 0.4749$ ($R^2 = 0.0011$);

670 $\ln K_d(Mn\text{-}Mg) = 0.5213 * NBO/T - 2.1634$ ($R^2 = 0.7408$);

671 $\ln K_d$(Cr-Mg) = 0.5706 * NBO/T - 2.4537 (R^2 = 0.7006);

672 $\ln K_d$(V-Mg): y = 0.8983 * NBO/T - 3.9291 (R^2 = 0.9112).

673 **Figure 5:** Comparison of D(Ni), D(Co), D(Mn), D(V), and D(Cr) to those from previous studies,
674 examining variations with D(Mg), NBO/T, and relative fO_2 (ΔFMQ).

675 **Figure 6:** Comparison of K_d(Ni-Mg), K_d(Co-Mg), K_d(Mn-Mg), K_d(Cr-Mg), and K_d(V-Mg)
676 from previous studies, examining variations with NBO/T.

677 **Figure 7:** Comparison of measured vs. predicted D(Ni), D(Co), D(Mn), D(V), and D(Cr)
678 olivine/melt. Predicted values were calculated using equations and constants tabulated in Table
679 4.

680 Data sources are listed in the legends, and also summarized in Table 4.

681 **Figure 8:** Difference between measured and calculated D(M) as a function of S content of
682 coexisting melt. D(M) olivine/melt predicted are calculated using equations summarized in Table
683 4. Shaded areas shows 2σ error on the predicted values.

684 **Figure 1**

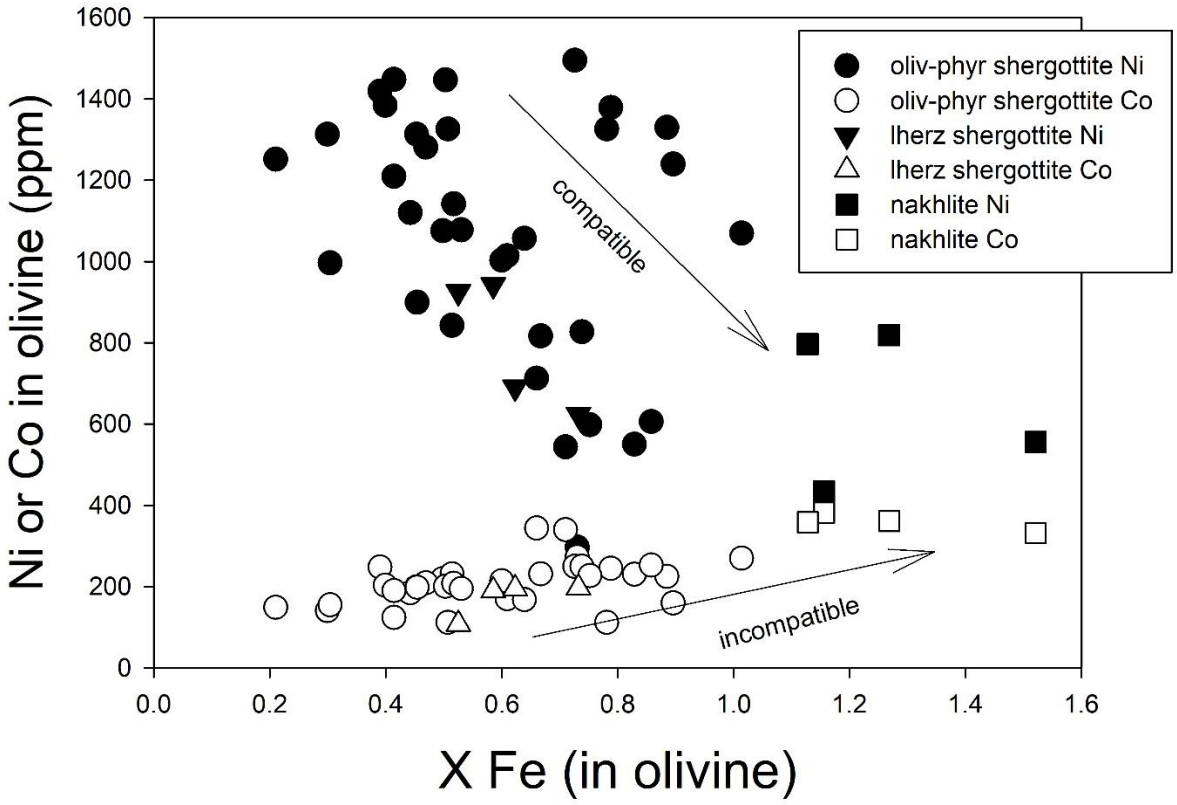

685

686

687 **Figure 2**

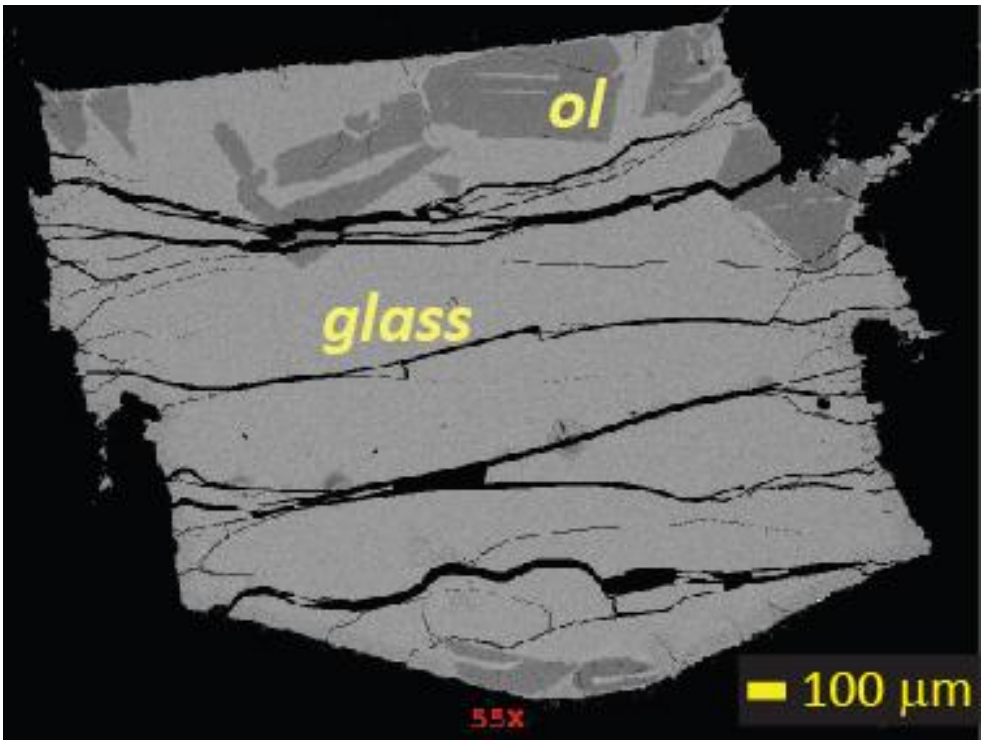

688

689

690 Figure 3:
691

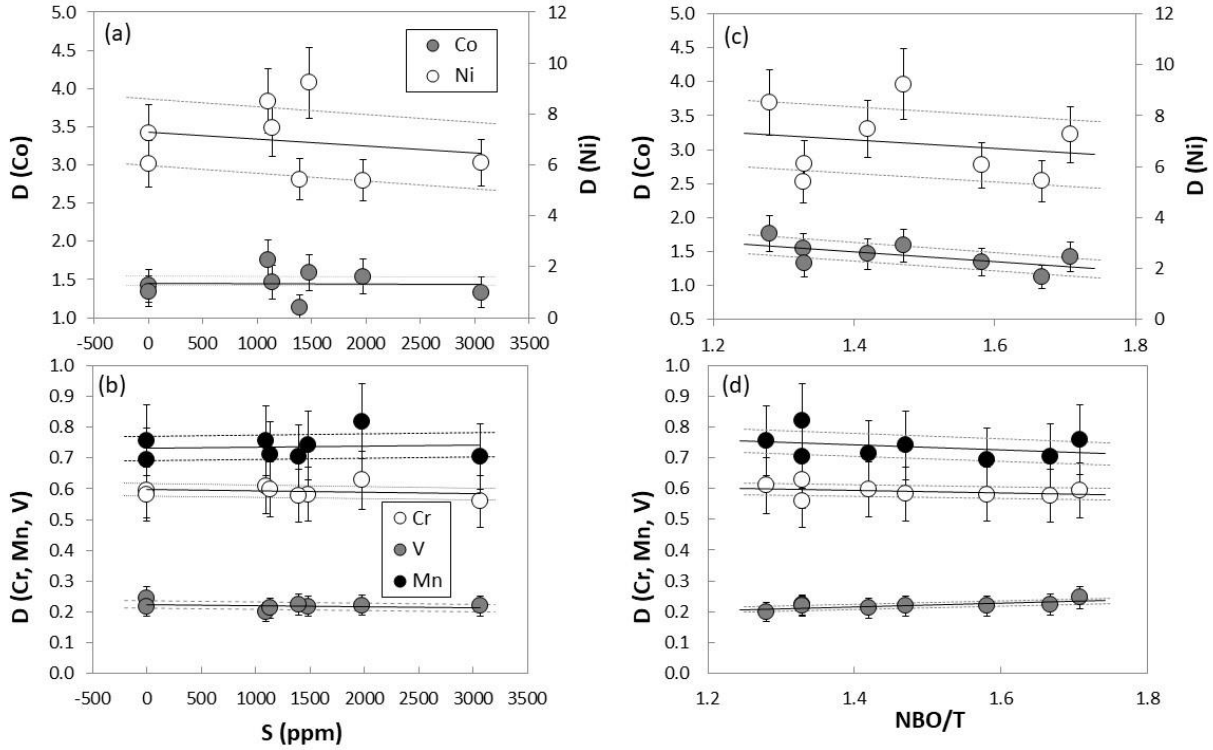

692
693
694

Figure 4:

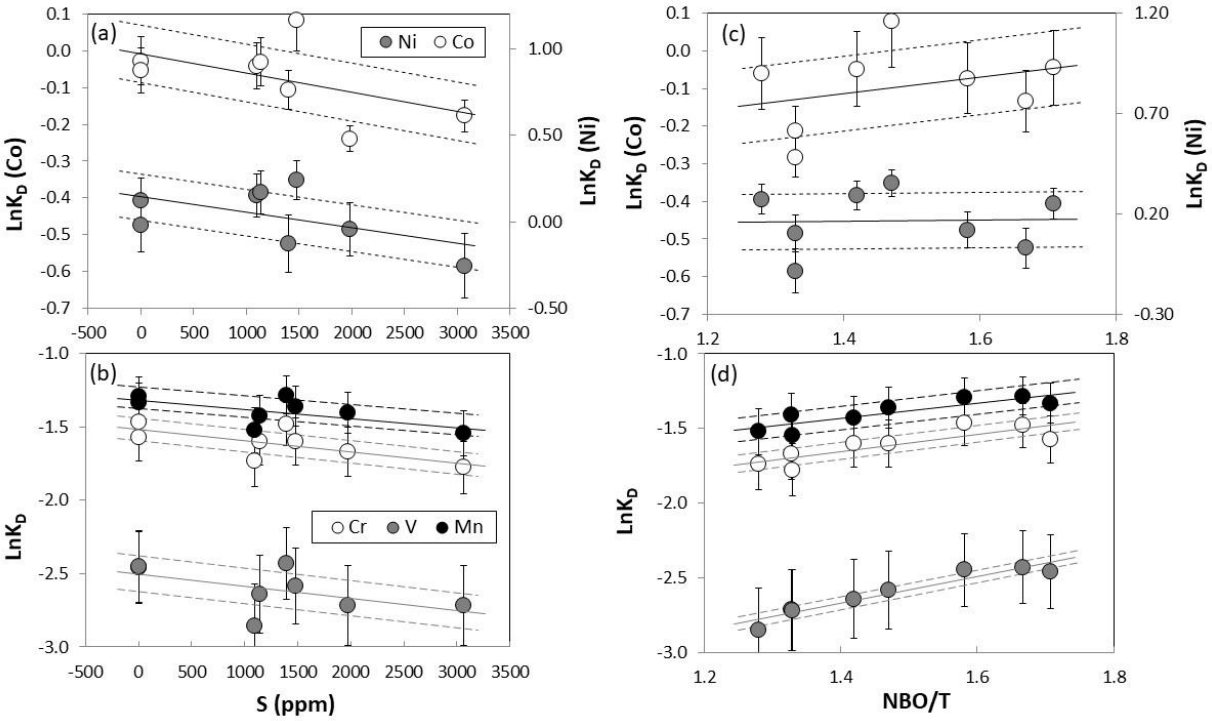

698 Figure 5:

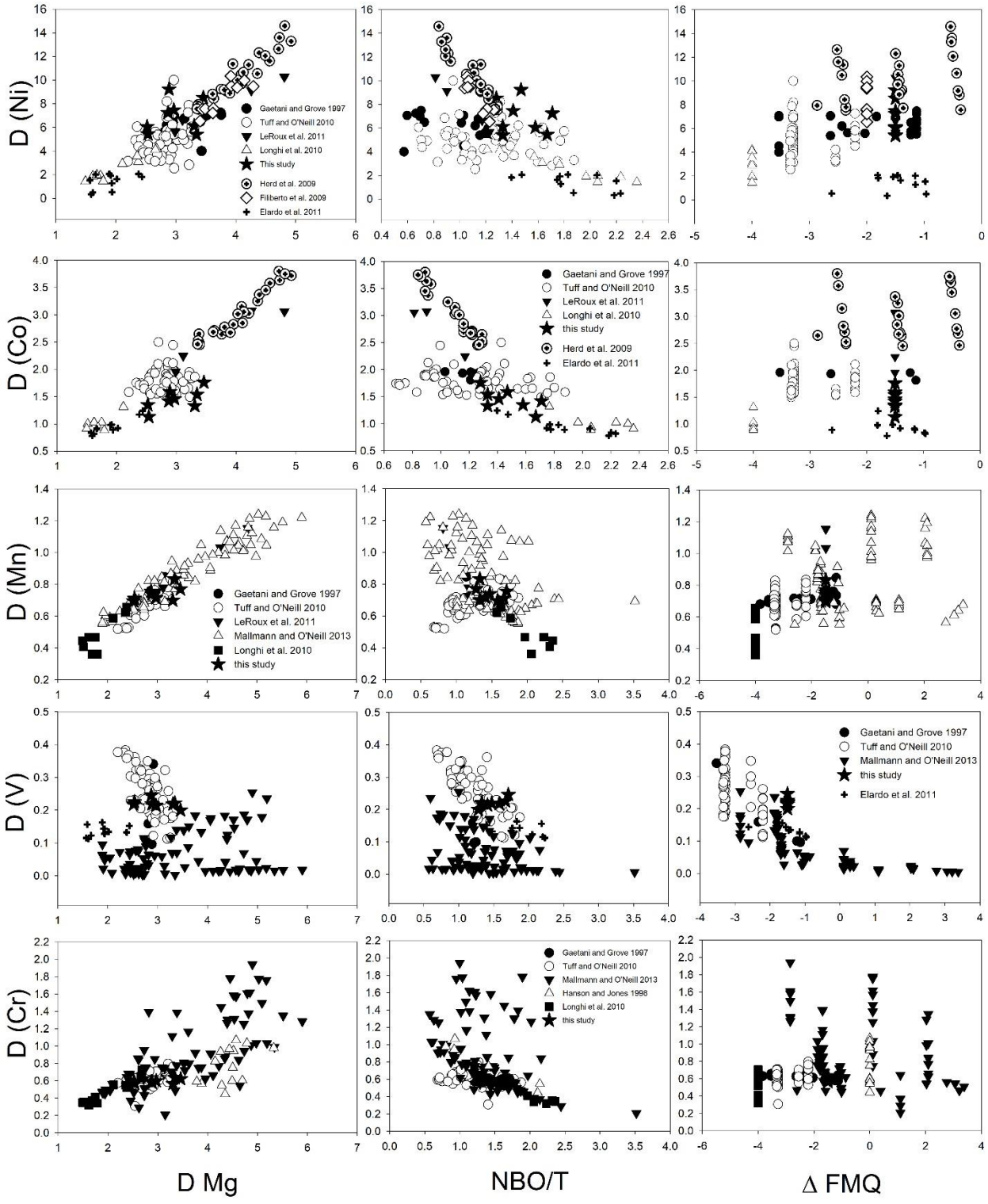

699

700

701

Figure 6:

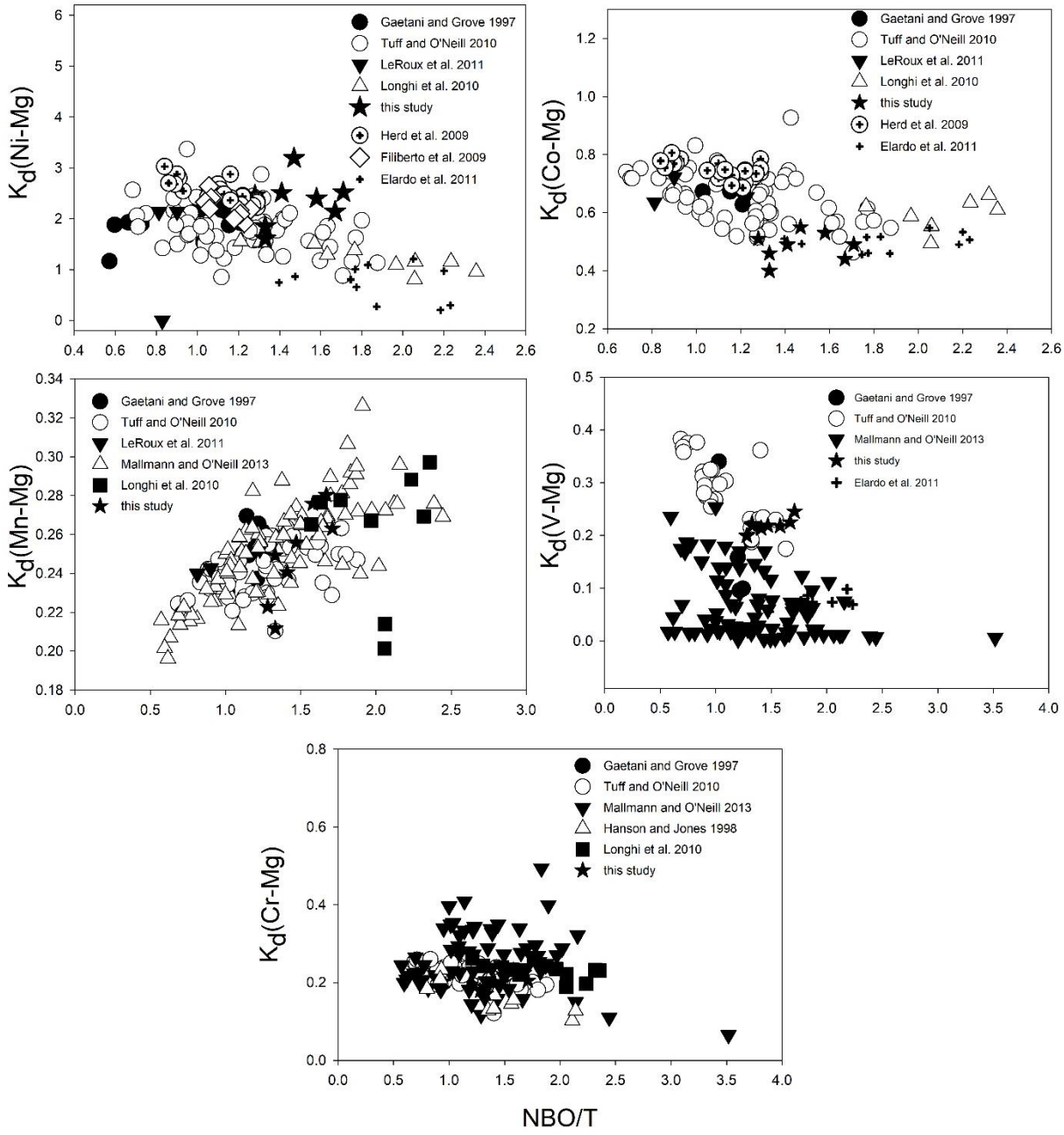

703

704

705

706 Figure 7:

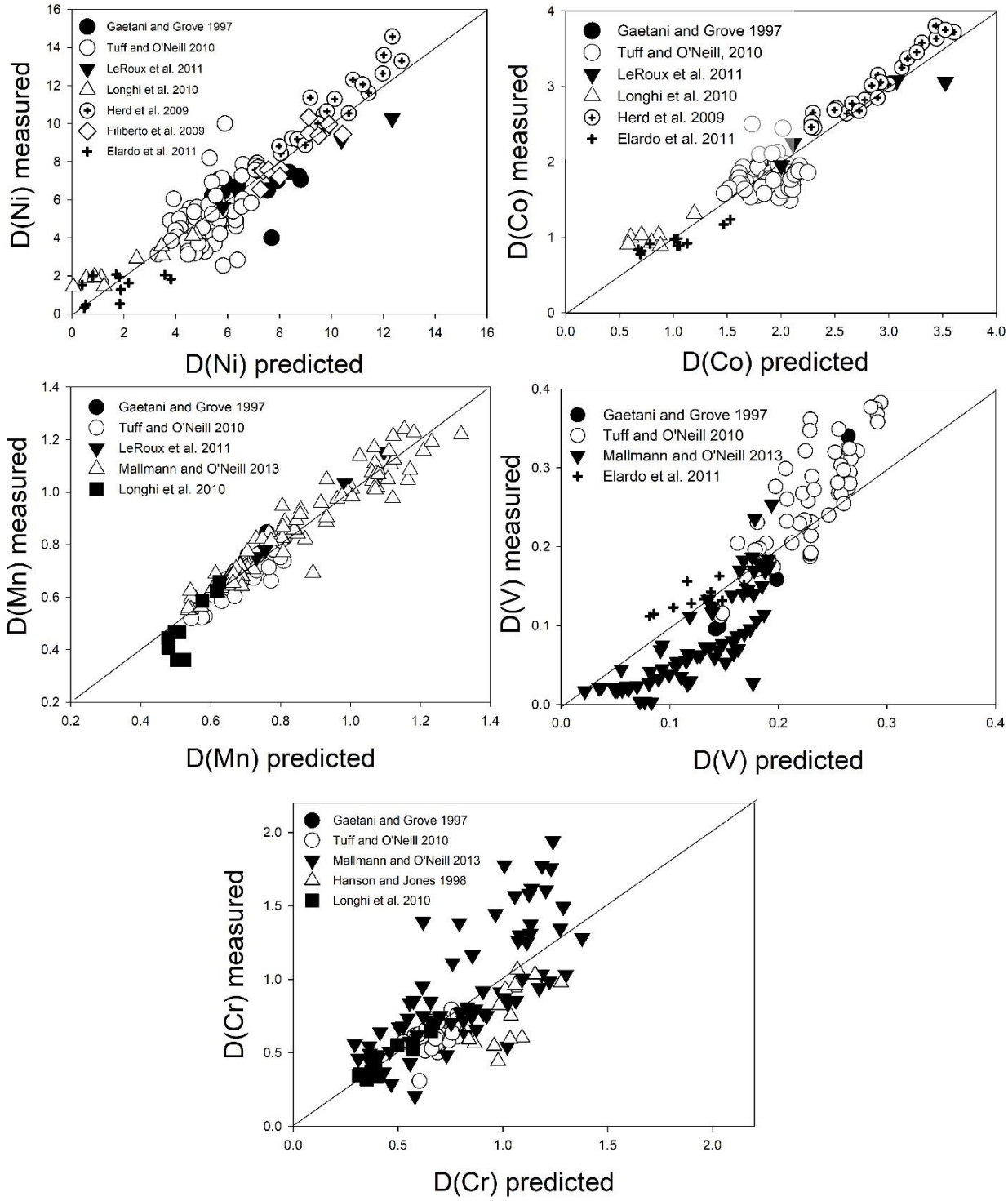

707
708

709 Figure 8:

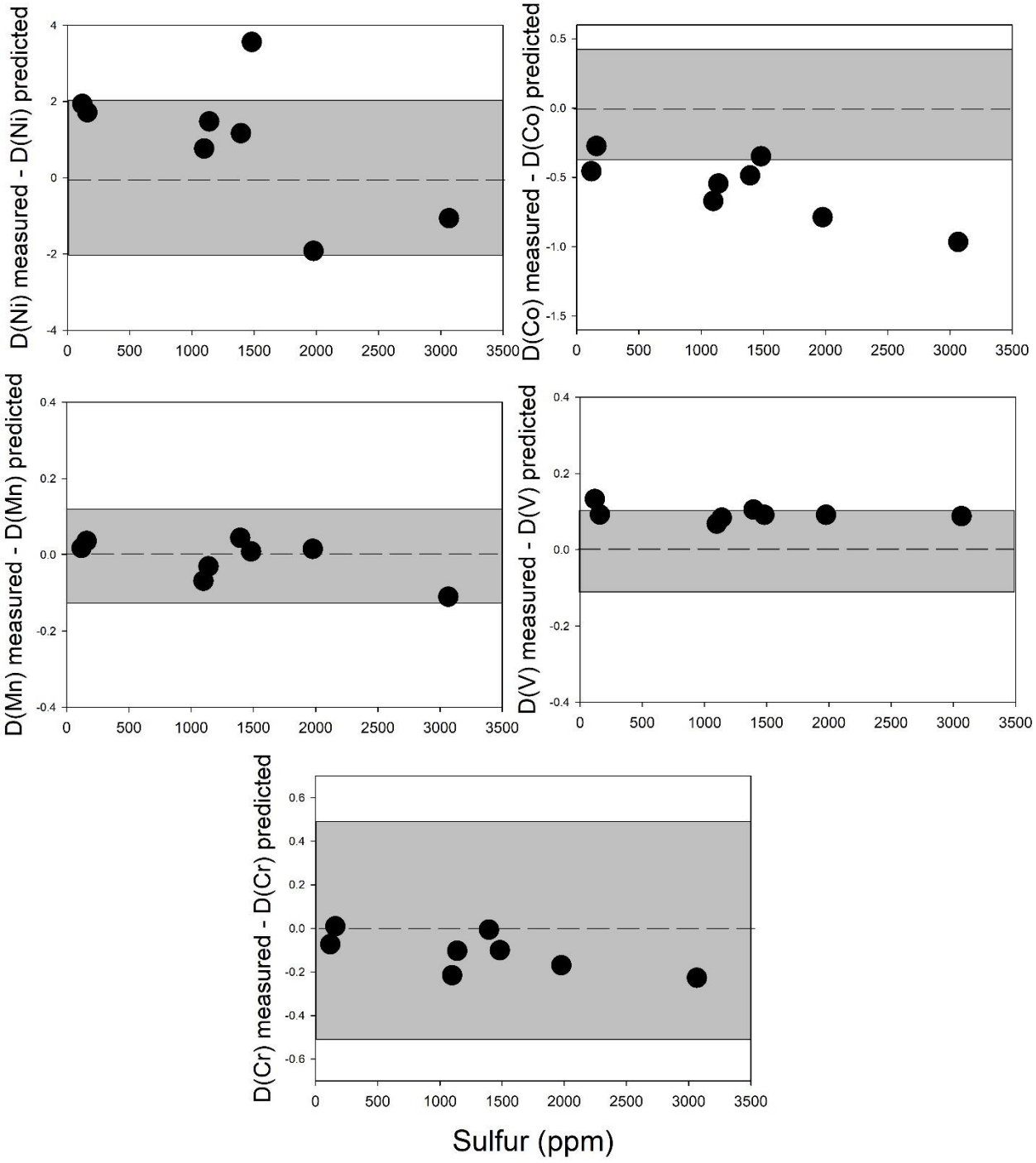

710
711
712

713 **Table 1: Run conditions, electron microprobe and SIMS analyses of glass** (all experiments at 0.75 GPa, with olivine and glass)
714

Run#	Starting	11	14	16	17	22	27	28	29
T (°C)		1500	1475	1475	1475	1450	1450	1450	1475
S added		2000	2000	1000	0	2000	0	1000	3000
% melt		98	93	88	98	85	88	83	86
n		13	12	12	10	12	13	14	12
SiO_2	49.9	46.81(40)	49.14 (20)	49.69(17)	49.24(43)	50.26(21)	49.74(30)	51.00(24)	50.31(36)
TiO_2	0.532	0.55(3)	0.55(3)	0.59(1)	0.51(1)	0.67(2)	0.62(3)	0.64(3)	0.62(2)
Al_2O_3	5.17	6.26(12)	6.62(30)	7.14(43)	6.24(6)	7.25(9)	7.03(14)	7.49(13)	7.49(10)
Cr_2O_3	0.659	0.65(3)	0.66(2)	0.67(2)	0.65(3)	0.68(2)	0.68(3)	0.63(2)	0.69(2)
FeO	17.3	16.83(19)	16.84(20)	16.55(30)	16.41(9)	16.70(17)	16.62(23)	16.59(16)	16.69(19)
MnO	0.481	0.45(4)	0.46(3)	0.49(4)	0.46(4)	0.42(3)	0.45(3)	0.48(2)	0.50(5)
MgO	18.7	17.58(32)	15.26(51)	14.82(58)	17.57(14)	12.87(12)	15.33(13)	12.65(19)	13.43(10)
CaO	6.83	6.98(13)	7.33(21)	7.76(17)	6.94(11)	7.98(6)	7.77(7)	8.17(9)	7.96(8)
Na_2O	0.651	0.70(3)	0.69(4)	0.78(3)	0.67(4)	1.30(5)	0.71(3)	0.79(3)	0.80(3)
K_2O	0.0156	0.024(14)	0.030(13)	0.028(10)	0.025(12)	0.030(13)	0.035(12)	0.038(11)	0.025(13)
P_2O_5	0.29	0.34(5)	0.34(7)	0.36(5)	0.32(4)	0.36(3)	0.33(4)	0.35(4)	0.36(4)
S (ppm)	-	1394(185)	1481(232)	1139(179)	160(131)	1977(267)	119(130)	1098(134)	3066(218)
Cr (ppm)	-	4416(203)	4487(125)	4556(166)	4468(202)	4664(130)	4621(176)	4330(166)	4710(142)
Mn (ppm)	-	3473(305)	3563(198)	3795(276)	3532(337)	3266(211)	3467(257)	3745(186)	3866(374)
Total	100.529	97.45(37)	98.22(45)	99.12(36)	99.08(53)	98.92(34)	99.35(44)	99.06(30)	99.50(46)
NBO/T	-	1.67	1.47	1.42	1.58	1.33	1.71	1.28	1.33
V (SIMS)	-	182(9)	188(10)	192(10)	187(10)	207(11)	201(10)	202(10)	192(10)
Co (SIMS)	-	437(22)	401(20)	385(19)	510(25)	316(16)	447(22)	358(17)	300(15)
Ni (SIMS)	-	71.0(4.0)	56.5(2.8)	56.7(2.8)	56.7(2.8)	39.7(2.0)	51.0(2.5)	43.1(2.2)	54.0(2.7)

Table 2: Olivine EMPA and SIMS analyses

Run#	11	14	16	17	22	27	28	29
n	11	11	13	11	11	13	15	15
SiO_2	39.13(10)	39.22(17)	39.21(15)	38.90(7)	38.75(9)	38.69(20)	38.45(26)	38.43(24)
Cr_2O_3	0.37(1)	0.38(1)	0.40(2)	0.38(1)	0.43(1)	0.40(1)	0.39(2)	0.39(2)
FeO	14.72(10)	16.08(24)	16.14(58)	14.77(6)	17.08(44)	15.82(26)	16.04(98)	15.43(74)
MnO	0.32(1)	0.34(1)	0.35(1)	0.32(1)	0.35(2)	0.34(1)	0.37(2)	0.35(2)
MgO	44.60(14)	44.08(29)	44.00(35)	44.31(11)	43.03(43)	44.03(22)	43.76(83)	44.41(67)
CaO	0.17(1)	0.17(1)	0.19(1)	0.18(1)	0.19(1)	0.18(1)	0.17(1)	0.17(1)
NiO	0.049(7)	0.066(12)	0.054(8)	0.044(8)	0.027(10)	0.047(9)	0.047(9)	0.042(10)
CoO	0.063(5)	0.081(7)	0.072(6)	0.087(5)	0.062(8)	0.081(6)	0.080(8)	0.051(5)
Total	99.43(27)	100.43(25)	100.41(39)	98.99(16)	99.91(14)	99.59(17)	99.30(14)	99.26(19)
Si	0.990	0.989	0.989	0.990	0.987	0.984	0.982	0.979
Cr	0.007	0.008	0.008	0.008	0.009	0.008	0.008	0.008
Fe^{2+}	0.312	0.339	0.340	0.314	0.364	0.336	0.343	0.329
Mn	0.0068	0.0073	0.0075	0.0068	0.0075	0.0073	0.0079	0.0076
Mg	1.683	1.657	1.655	1.681	1.634	1.669	1.666	1.687
Ca	0.0047	0.0046	0.0051	0.0050	0.0051	0.0050	0.0047	0.0046
Ni	0.0010	0.0013	0.0011	0.0009	0.0006	0.0010	0.0010	0.0009
Co	0.001	0.002	0.001	0.002	0.001	0.002	0.002	0.001
Total	3.0	3.0	3.0	3.0	3.0	3.0	3.0	3.0
Fo	83.8(1)	82.4(3)	82.3(6)	83.6(1)	81.2(5)	82.6(3)	82.3(1.1)	83.1(9)
Mg #	84.4(1)	83.0(3)	82.9(6)	84.2(1)	81.8(5)	83.2(3)	83.2(3)	83.7(9)
V (SIMS)	41.0(4.0)	41.1(4.1)	41.0(4.0)	40.8(4.1)	45.8(4.6)	49.4(5.0)	40.2(4.0)	41.9(4.2)
Co (EMPA)	493(25)	636(32)	563(28)	686(34)	486(24)	635(32)	629(31)	399(20)
Ni (EMPA)	386(19)	521(26)	423(21)	343(17)	214(11)	369(18)	367(18)	331(16)

717

718 **Table 3: D and K_d values**

Run #	**27**	**28**	**22**	**17**	**16**	**14**	**29**	**11**
Temp	1450	1450	1450	1475	1475	1475	1475	1500
S (ppm)	0	1000	2000	0	1000	2000	3000	2000
D V	0.25(3)	0.20(3)	0.22(3)	0.22(3)	0.21(3)	0.22(3)	0.22(3)	0.23(3)
D Cr	0.60(4)	0.62(4)	0.63(4)	0.58(4)	0.60(4)	0.58(4)	0.57(4)	0.57(4)
D Mn	0.76(9)	0.77(9)	0.83(9)	0.70(8)	0.71(8)	0.74(8)	0.70(8)	0.71(8)
D Fe	0.95(2)	0.97(2)	1.02(2)	0.90(2)	0.98(2)	0.96(2)	0.92(2)	0.87(2)
D Co	1.42(14)	1.76(18)	1.54(15)	1.35(14)	1.46(15)	1.59(16)	1.33(13)	1.13(12)
D Ni	7.24(73)	8.52(85)	5.39(55)	6.05(61)	7.46(75)	9.22(92)	6.13(63)	5.44(60)
D Mg	2.87(5)	3.46(5)	3.34(5)	2.52(5)	2.97(5)	2.89(5)	3.31(5)	2.54(5)
K_d (V-Mg)	0.085(10)	0.058(10)	0.066(10)	0.086(10)	0.072(10)	0.076(10)	0.066(10)	0.088(10)
K_d (Cr-Mg)	0.20(3)	0.18(2)	0.19(2)	0.23(3)	0.20(2)	0.20(2)	0.17(2)	0.22(3)
K_d (Mn-Mg)	0.26(3)	0.22(3)	0.25(3)	0.28(3)	0.24(3)	0.26(3)	0.21(2)	0.28(3)
K_d (Fe-Mg)	0.33(1)	0.28(1)	0.31(1)	0.36(1)	0.33(1)	0.33(1)	0.28(1)	0.35(1)
K_d (Co-Mg)	0.49(6)	0.51(5)	0.46(5)	0.53(6)	0.49(5)	0.55(6)	0.40(5)	0.44(5)
K_d (Ni-Mg)	2.52(26)	2.46(25)	1.61(17)	2.40(25)	2.51(26)	3.19(32	1.85(20)	2.14(22)

719 **Table 4: Regression results for D(olivine/melt):** $D = a\ D(Mg) + b\ NBO/T + c\ \Delta FMQ + d\ (S\ ppm) + e$

Element	a	b	c	d	E	N	Std error	Studies
Ni	3.23(19)	-1.29(43)	-	-	-1.78(1.09)	82	1.00	2,3,4,5,6,7
Co	0.805(38)	-0.182(85)	-	-	-0.124(219)	69	0.20	2,3,4,5,7
Co (with S)	0.495(67)	-0.311(91)	-	-0.0000824 (253)	0.843(267)	117	0.23	1,2,3,4,5,7,8
Mn	0.206(6)	0.045(12)	-	-	0.0689(319)	121	0.054	2,3,4,9
V	-0.0619(123)	-0.0140(58)	-0.0398(29)	-	0.199(33)	116	0.051	2,7,9
Cr	-0.0448(578)	0.262(29)	-0.0404(139)	-	-0.0752(167)	113	0.252	2,4,9,10

720

721 1 – Gaetani and Grove, 1997; 2 – Tuff and O'Neill, 2010; 3 – LeRoux et al., 2011; 4 – Longhi et al., 2010; 5 – Herd et al., 2009; 6 –
722 Filiberto et al., 2009; 7 – Elardo et al., 2011; 8 – this study; 9 – Mallmann and O'Neill, 2013; 10 – Hanson and Jones, 1998.